Magnetoconductance of carbon nanotubes

M. F. Lin and Kenneth W.-K. Shung
Physics Department, National Tsing Hua University, Hsinchu, Taiwan 30043, The Republic of China
(Received 19 September 1994)

As a result of the interaction between the spin and the magnetic field (B), special step structures are predicted to exist in the ballistic magnetoconductance of carbon nanotubes. The electronic structure of a carbon nanotube drastically changes from a metal (semiconductor) to a semiconductor (metal) during the variation of the magnetic flux. When the spin-B interaction is neglected, the Fermi level only touches the conductance and valence bands of a metallic nanotube. This paramagnetic interaction could make the subbands cross and intersect with the Fermi level within a certain magnetic-flux range; the ballistic magnetoconductance thus exhibits step structures. Such special structures are expected to be observable at low temperature (<1 K) and bias voltage (<0.1 mV). Moreover there exists another effect, the doping effect, which could lead to step structures even without the spin-B interaction.

Iijima[1] recently reported the observation of carbon nanotubes, which are graphite sheets rolled up in the cylindrical form. These nanotubes, with radii between 10 and 150 Å, represent a new class of quasi-one-dimensional systems. They have attracted many recent studies.[2–10] One of the studies, made by Tian and Datta,[10] addressed the interesting transport properties. The authors mainly discussed the effects of finite bias voltages and of finite temperatures on magnetoconductance [$G(\phi)$]. In this work we further introduce both the interaction between the spin and the magnetic field (B) and the doping effect and predict steplike structures in ballistic magnetoconductance at vanishing bias voltage and temperature.

Quantization conductance in the low-dimensional system was first proposed by Landauer.[11] This special phenomenon has stirred considerable recent attention on quantum narrow constrictions, e.g., quantum wires[12,13] and quantum dots.[14,15] It has been identified by experimental[16,17] measurements on the quantum constrictions in GaAs microstructures. The carbon nanotubes closely resemble cylindrical quantum wires. For three-dimensional (3D) cylindrical microwires, Bogachek *et al.*[13] calculated the ballistic $G(\phi)$ (without any scattering in the sample), which is proportional to the number of current-carrying modes intersecting the Fermi level. At vanishing bias voltage and temperature, they obtained many magnetic-flux-induced conductance steps within one fundamental magnetic flux ϕ_0 ($=hc/e$), which is due to many transverse current-carrying modes being switched on or off. Here each carbon nanotube is a hollow cylinder and so there are one or two step structures (corresponding to four active modes) within one ϕ_0. But carbon nanotubes may consist of N-shell nanotubes. This special coaxial structure makes carbon nanotubes exhibit many step structures in $G(\phi)$, as 3D quantum microwires do.

The band property, metal or semiconductor, of a carbon nanotube was predicted to rely on the radius and the chiral structure about the axis.[4–7] We consider carbon nanotubes with any chiral angles existing in uniform B field along the tubular axis. Their electronic structures are calculated by the tight-binding model in the absence of the intertube interaction. Each carbon nanotube could drastically change from a metal (semiconductor) to a semiconductor (metal) during the variation of ϕ. The energy dispersion without the spin-B interaction is periodic in ϕ, with a period ϕ_0, as a result of the Aharonov-Bohm (AB) effect. There is no step structure[10] in $G(\phi)$ under such condition [i.e,. the with of $G(\phi)$ is zero] because the Fermi level only touches the conduction and valence bands at a creation ϕ. The spin-B interaction is currently taken into account in calculating $G(\phi)$. This paramagnetic interaction makes the subbands capable of crossing the Fermi level within a certain magnetic-flux range.[18] Magnetoconductance of the ballistic carbon nanotubes is thus expected to show step structures. $G(\phi)$ is calculated at various temperatures (T) and bias voltages (V) to see under which condition step structures are observable.

There is another effect that could result in step structures in $G(\phi)$. It is the intercalation of metallic atoms[7] (e.g., K, Rb, and Cs) into the carbon nanotubes. Electrons will be transferred from the metallic atoms to the carbon nanotubes, as found in graphite intercalation compounds (GIC's) and carbon fibers.[19] Therefore, the Fermi energy (E_F) would increase from zero to a finite value. There are many current-carrying modes intersecting the Fermi level under the doped case. The doped nanotubes will exhibit step structures when the conduction bands cross the Fermi level to become vacant or occupied. There are eight step structures within ϕ_0 for a single-shell nanotube. The step structures depending on E_F are available at very small ϕ. This implies that the experimental measurements may be easier to perform.

We first present the electronic structure of the carbon nanotube which exists in a uniform B field along the tubular axis. The geometric structure of a carbon nanotube, as shown in Fig. 1(a), can be built from a graphite sheet. A carbon nanotube is formed by rolling the sheet in such a fashion that the atom at the origin coincides with another atom at $\mathbf{R}_x = m\mathbf{a}_1 + n\mathbf{a}_2$, where $\mathbf{a}_1 = \sqrt{3}b\mathbf{e}_{x'}$ and $\mathbf{a}_2 = (\sqrt{3}b/2)\mathbf{e}_{x'} - (3b/2)\mathbf{e}_{y'}$. $\mathbf{a}_1$ and $\mathbf{a}_2$ are the primi-

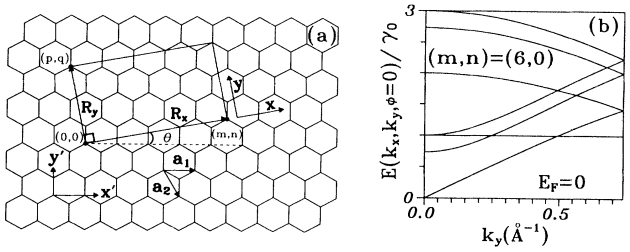

FIG. 1. (a) A carbon nanotube is just a graphite sheet rolled from the origin to the vector $\mathbf{R}_x=m\mathbf{a}_1+n\mathbf{a}_2$. The tubular axis is parallel to the primitive vector $\mathbf{R}_y$ $(=p\mathbf{a}_1+q\mathbf{a}_2)$ of the unrolled nanotube. The x' axis and the y' axis are relative to the graphite sheet. The x axis and the y axis are parallel to $\mathbf{R}_x$ and $\mathbf{R}_y$, respectively. (b) The conduction bands of the (6,0) nanotube. The valence bands are symmetric, about $E_F=0$, to the conduction bands.

tive lattice vectors of the graphite sheet, $\mathbf{e}_{x'}$ $(\mathbf{e}_{y'})$ is the unit vector along the x' (y') axis, and $b=1.42$ Å is the nearest-neighbor distance. The nanotube so obtained clearly is fully determined by the pair of the parameters (m,n). The chiral angle of this tubule, $\theta=\tan^{-1}[-\sqrt{3}n/(2m+n)]$, is defined to be the angle between the vector $\mathbf{R}_x(\|\mathbf{e}_x)$ and the zigzag $(\mathbf{e}_{x'})$ direction. The radius of the carbon nanotube is $r=|\mathbf{R}_x|/2\pi=b\sqrt{3(m^2+mn+n^2)}/2\pi$. (m,n) is used to represent any lattice vector $\mathbf{R}_x$ or carbon nanotube. Also shown in Fig. 1(a) is the primitive vector $\mathbf{R}_y$ of the unrolled nanotube along the axial direction $(\|\mathbf{e}_y)$. $\mathbf{R}_y$ denoted by (p,q) is perpendicular to $\mathbf{R}_x$; therefore, (p,q) gives the smallest $\mathbf{R}_y$ and satisfies $p(2m+n)+q(m+2n)=0$. The transverse and axial directions are parallel to $\mathbf{e}_x$ and $\mathbf{e}_y$, respectively, and so the coordinate system (x,y) is relatively convenient in expressing the electronic structure in the presence of the B field.

An unrolled carbon nanotube is just a graphite sheet with the boundary condition along the transverse direction and the translational symmetry along the axial direction. The electronic structure of the carbon nanotube here is calculated by the tight-binding model, which is similar to that employed for a graphite sheet,[20] but with the boundary condition along the transverse direction taken into account. The boundary condition depends on the uniform B field parallel to the tubular axis. The gauge $\mathbf{A}=\mathbf{B}\times\mathbf{r}/2$ $(\|\mathbf{e}_x)$ is chosen such that wave vector is $\mathbf{k}=-i\nabla+(e/c\hbar)\mathbf{A}$. The boundary condition under such gauge is $\Psi(\mathbf{r}+\mathbf{R})=\Psi(\mathbf{r})$, where $\Psi(\mathbf{r})$ is the Bloch function. By the detailed calculations,[18] the energy dispersion of the (m,n) carbon nanotube is given by

$$E(k_x,k_y,\sigma,\phi)=E(k_x,k_y,\phi)+E(\sigma,\phi)\ , \tag{1a}$$

where

$$E(k_x,k_y,\phi)=\pm\gamma_0\left\{1+4\cos\left[\frac{3b}{2}(k_y\cos\theta+k_x\sin\theta)\right]\cos\left[\frac{\sqrt{3}b}{2}(k_y\sin\theta-k_x\cos\theta)\right]+4\cos^2\left[\frac{\sqrt{3}b}{2}(k_y\sin\theta-k_x\cos\theta)\right]\right\}^{1/2} \tag{1b}$$

and

$$E(\sigma,\phi)=\frac{g\sigma}{m^*r^2}\frac{\phi}{\phi_0}\ . \tag{1c}$$

The transverse wave vector obtained from the boundary condition is $k_x=2\pi(J+\phi/\phi_0)/b\sqrt{3(m^2+mn+n^2)}$ $(J=1,2,\ldots,N_u/2)$. The positive integer J corresponding to k_x serves as the angular momentum or the subband index. N_u $[=4\sqrt{(p^2+pq+q^2)(m^2+mn+n^2)/3}]$ is the total electron number within the rectangle bounded by $\mathbf{R}x$ and $\mathbf{R}_y$. The axial wave vector $|k_y|\le\pi/b\sqrt{3(p^2+pq+q^2)}$ is confined within the first Brillouin zone. The spin-B interaction $E(\sigma)=(g\sigma/m^*r^2)(\phi/\phi_0)$ is very important here since it clearly changes the characteristic of the magnetoconductance (see later). The g factor is taken to be the same as that $(\simeq 2)$ of the pure graphite or GIC's.[19] $\sigma=\pm\frac{1}{2}$ is the electron spin and m^* is the bare electron mass.

The form of the energy dispersion is relatively simple for two types of carbon nanotubes: zigzag type $(\theta=0°)$ and armchair type $(\theta=\pm 30°)$.[6] Their respective energy dispersions, without the spin-B interaction, are

$$E(k_x,k_y,\phi)_{\text{zigzag}}=\pm\gamma_0\left\{1+4\cos\left[\frac{3bk_y}{2}\right]\cos\left[\frac{\sqrt{3}bk_x}{2}\right]+4\cos^2\left[\frac{\sqrt{3}bk_x}{2}\right]\right\}^{1/2} \tag{2a}$$

and

$$E(k_x,k_y,\phi)_{\text{armchair}}=\pm\gamma_0\left\{1+4\cos\left[\frac{\sqrt{3}bk_y}{2}\right]\cos\left[\frac{3bk_x}{2}\right]+4\cos^2\left[\frac{\sqrt{3}bk_y}{2}\right]\right\}^{1/2}\ , \tag{2b}$$

where both $(\sqrt{3}bk_x/2)_{\text{zigzag}}$ and $(3bk_x/2)_{\text{armchair}}$ are equal to $(\pi/m)(J+\phi/\phi_0)$ $(J=1,2,\ldots,2m)$. All of the armchair nanotubes are metals at $\phi=0$.

At $\phi=0$, the (m,n) nanotube with $2m+n=3\mathcal{J}$ $(\neq 3\mathcal{J}$, where $\mathcal{J}$ is an integer) is metallic (semiconducting),[6] as obtained from Eq. (1a). For example, the (6,0) zigzag nanotube is a metal. Its electronic structure, in which all of the subbands are doubly degenerate except those two with $J=m$ and $2m$, is given in Fig. 1(b). Both conduc-

tion and valence bands are symmetric about the Fermi level $E_F=0$. The electronic structure varies with the nonzero magnetic flux through the nanotube. It is periodic in ϕ, with a period ϕ_0, if the spin-B interaction is neglected. A carbon nanotube with $2m+n=3\mathcal{J}$ ($\neq 3\mathcal{J}$) is thus metallic at $\phi_a=\mathcal{J}\phi_0$ [$(\mathcal{J}\pm\frac{1}{3})\phi_0$]; otherwise, it is semiconducting. Under such conditions, the Fermi level only touches the conduction and valence bands at ϕ_a. But when the spin-B interaction is taken into account, the subbands closest to the Fermi level could cross it at the neighborhood of ϕ_a.[18] This means that a carbon nanotube is a metal within a certain magnetic-flux range near ϕ_a. This special feature of the electronic structure due to the spin-B interaction could result in step structures in the ballistic magnetoconductance.

We consider an N-shell tubular system suspended between two macroscopic leads (reservoirs) and calculate the magnetoconductance in the ballistic regime. Here the current flowing down the carbon nanotubes is driven by the bias voltage V between two leads. There is no scattering in the ballistic carbon nanotubes, but the elastic scattering of electrons at the contacts between nanotubes and leads is assumed to be very strong. By the detailed derivations,[13] the current is given by

$$I(\phi)=eT_0\sum_{k_x,\sigma;N_1}\int_{k_y>0}\frac{dk_y}{2\pi}\frac{1}{\hbar}\left|\frac{\partial E}{\partial k_y}\right|\{f^0(E-\mu-eV)-f^0(E-\mu)\}_{E=E(k_x,k_y,\sigma,\phi;N_1)}, \tag{3}$$

where $1/\hbar|\partial E/\partial k_y|$ is the longitudinal velocity. T_0 [see Eq. (4) in Ref. 13] is the net probability for electrons in the reservoirs entering the carbon nanotubes with the velocity $1/\hbar|\partial E/\partial k_y|$ and is just equal to 1 for the adiabatic contacts. f^0 is the Fermi-Dirac distribution function and $E(k_x,k_y,\sigma,\phi;N_1)$ is the energy dispersion of the N_1th nanotube in the absence of the intertube interaction. μ and $\mu+eV$ are chemical potentials of the two reservoirs. μ is the same as the Fermi energy E_F of carbon nanotubes at $V=0$ mV. We still take $\mu=E_F$ for $V\neq 0$ mV in the calculations, although the chemical potential only needs to satisfy the conditions $eV+\mu\geq E_F$ and $\mu\leq E_F$.

Equation (3) is useful in calculating the magnetoconductance defined by $G(\phi)=I(\phi)/V$. At vanishing bias voltage, the expression of $G(\phi)$ is reduced to

$$G(\phi)=\frac{-e^2T_0}{h}\sum_{k_x,\sigma;N_1}\int_{k_y>0}dk_y\left|\frac{\partial E}{\partial k_y}\right|\frac{\partial f^0(E)}{\partial E_{|E=E(k_x,k_y,\sigma,\phi;N_1)-\mu}}. \tag{4}$$

$\partial f^0(E)/\partial E$ is a delta function $\delta(E)$ at zero temperature. $G(\phi)$ is thus proportional to the number of current-carrying states intersecting with the Fermi level, which is the so-called quantization conductance. There exists one step structure in $G(\phi)$ when one current-carrying state is switched on or off. The step structures in $G(\phi)$ may disappear at high temperatures and bias voltages because of the broadening effects.

We discuss first the result of the single-shell system. The zigzag (210,0) nanotube is chosen for a model study because the special step structure in $G(\phi)$ is relatively easily understood from its simple energy dispersion in Eq. (2a) and there is no loss of generality. The (210,0) nanotube has a radius $r=82.22$ Å and the B field corresponding to ϕ_0 is 19.47 T. $G(\phi)$ of the (210,0) nanotube is shown in Fig. 2 at $T=0$ K and $V=0$ mV. $G(\phi)$ (normalized to e^2T_0/h) is just the number of the active states intersecting the Fermi level $E_F=0$. The circle-dashed curve is the result in which the spin-B interaction is neglected. $G(\phi)=4$ only shows at $\phi=\mathcal{J}\phi_0$, where the (210,0) nanotube is a metal in the absence of the spin-B interaction; otherwise, $G(\phi)=0$. It is a periodic function with a period ϕ_0, due to the AB effect. The periodicity of the AB effect is independent of temperature and bias voltage,[10] but is apparently destroyed by the inclusion of th spin-B interaction, as shown by the solid curve. Due to the effect of Zeeman splitting, there exists a special structure (step) in $G(\phi)$ at the neighborhood of ϕ_0. The other step structures are located at the positions close to $2\phi_0, 3\phi_0, \ldots$ (not shown). Their positions correspond to the semiconductor-metal transitions during the variation of the electronic structure with the magnetic flux, i.e., they are close to $\mathcal{J}\phi_0$ for a carbon nanotube with $2m+n=3\mathcal{J}$.

$G(\phi)$ close to ϕ_0 deserves a closer examination. If the

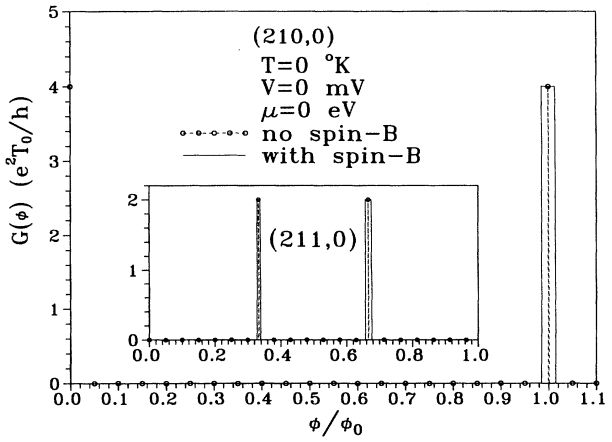

FIG. 2. Magnetoconductance $G(\phi)$ of the (210,0) nanotube at $T=0$ K, $V=0$ mV, and $\mu=0$ eV. The circle-dashed and solid curves are, respectively, calculated without and with spin-B interactions. Also shown in the inset for comparison is $G(\phi)$ of the (211,0) nanotube.

spin-B interaction is neglected, the bottoms ($k_y=0$) of the subbands denoted by $J_a=139$ and 279 only touch the Fermi level at $\phi=\phi_0$. $G(\phi)$ in the circle-dashed curve is thus a single point with height of 4 at $\phi=\phi_0$. These two conduction (valence) bands with spin-down (spin-up) states could cross the Fermi level by including the spin-B interaction. When their band bottoms ($k_y=0$) begin to cross the Fermi level at $0.9858\phi_0$, the two conduction (valence) bands become occupied (vacant). It remains so until $\phi \geq 1.0145\phi_0$. Therefore, there are four current-carrying states from two conductance bands and two valence bands at $0.9858\phi_0 \leq \phi \leq 1.0145\phi_0$. Under the condition of the crossing of Fermi level, the crossing position ϕ_c should satisfy $|E(J_a,k_y=0,\phi_c)_{\text{zigzag}}| = |(g\sigma/m^*r^2)(\phi_c/\phi_0)|$. Hence the width w of the step structure from the difference of the two crossing positions is approximately given by[18]

$$w \approx \frac{4\phi_a}{3b\gamma_0\phi_0}\left|\frac{g\sigma}{m^*r}\right| . \tag{5}$$

The step width in the solid curve is about $0.0287\phi_0$. The approximate expression of w in Eq. (5) is also suitable for a carbon nanotube with any chiral angle, as estimated from Eqs. (1a)–(1c). The step width in $G(\phi)$ is proportional to ϕ_a, at which a carbon nanotube is metallic in the absence of the spin-B interaction. Moreover Eq. (5) implies that if two different nanotubes have the same radius and ϕ_a, they will exhibit the same step structure in $G(\phi)$.

Another kind of nanotube with $2m+n \neq 3\mathcal{J}$, for example, a (211,0) nanotube, is shown in the inset of Fig. 2 for comparison. The step structures of the (211,0) nanotube are very different from those of the (210,0) nanotube, e.g, height, position, and width. Here the step structures in $G(\phi)$ with a height of 2 center at the neighborhood of $\frac{1}{3}\phi_0$ and $\frac{2}{3}\phi_0$, whose widths are $0.0095\phi_0$ and $0.0191\phi_0$, respectively. The step structure near $\frac{1}{3}\phi_0$ ($\frac{2}{3}\phi_0$) comes form $J_a=281$ ($J_a=140$) subbands crossing and intersecting with the Fermi level. Hence there are two current-carrying states which include one spin-down state in the conductance band and one spin-up state in the valence band in each step structure. We present only the results of two zigzag nanotubes, respectively, belonging to different kinds of tubules, but the basic features, height, position, and width of the step structures are similar to those in Fig. 2 for other nanotubes. We could make a simple conclusion: a carbon nanotube with $2m+n=3\mathcal{J}$ ($\neq 3\mathcal{J}$) exhibits step structures with a height of 4 (2) at ϕ close to $\phi_a=\mathcal{J}\phi_0$ [$(\mathcal{J}\pm\frac{1}{3})\phi_0$], whose widths are described by Eq. (5).

For a multiple-shell system, we neglect the modification of the intertube interaction to the electronic structure and the magnetoconductance. The total current-carrying states intersecting the Fermi level is the sum of those coming from the independent carbon nanotubes. $G(\phi)$ of the N-shell system is shown in Fig. 3 at $T=0$ K and $V=0$ mV. $N=1$, 2, 5, 10, and 20, and $N=1$ stands for the (210,0) nanotube. The result shows that there are more step structures for a larger N, as expected from Eq. (4). Moreover the step structures could occur at the smaller B field, e.g., the $N=20$ system. A tubular system with more shells is thus more suitable for observing the special step structures in $G(\phi)$. The nanotubes used in the calculations are chosen to satisfy the necessary condition: the distance between two nearest nanotubes is limited to 3.35–3.40 Å. We additionally confine the chiral angle to $-30° \leq \theta \leq 0°$, i.e., $m \geq n \geq 0$. All of the nanotubes are thus metallic ($2m+n=3\mathcal{J}$) at $\phi=0$, except the third nanotube ($2m+n\neq 3\mathcal{J}$). In fact, most of the nanotubes in the multiple-shell system are metallic (belonging to the armchair nanotubes), if the intertube distances are as described above. When (m,n), representing a carbon nanotube, is known, we could easily understand each step structure, as stated in the preceding paragraph. For example, the two step structures with a height of 2 in the $N=5$ system are due to the third nanotube.

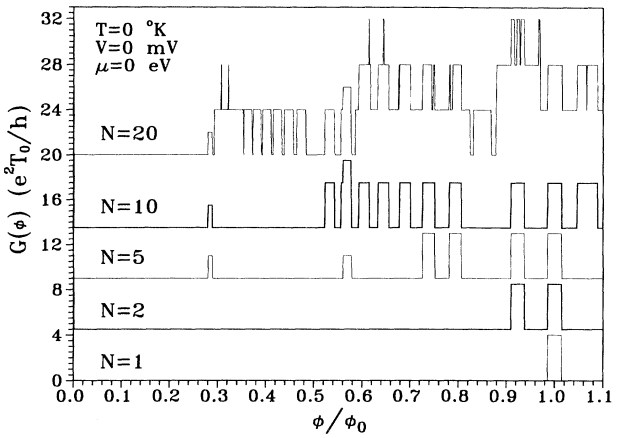

FIG. 3. $G(\phi)$ of the N-shell nanotubes at $T=0$ K, $V=0$ mV, and $\mu=0$ eV. $N=1$, 2, 5, 10, and 20 and $N=1$ corresponds to the (210,0) nanotube. ϕ/ϕ_0 is normalized to that of the (210,0) nanotube. For visual convenience, different weights have been added to each curve, i.e., $G(\phi)$ in all of the curves should be equal to 0 at the small ϕ's.

We further study the broadening effects due to finite temperatures and finite bias voltages and under which condition the step structure in $G(\phi)$ could be observed by the experimental measurements. $G(\phi)$ of the (210,0) nanotube is shown in Fig. 4 at various T's and $V=0$ mV. The step structure close to ϕ_0 is gradually broadened by the increasing temperature and it is completely buried by the thermal broadening at $T \geq 10$ K. The cause of the disappearance is that the magnitude of the spin-B interaction (~ 1 meV) corresponds to the thermal energy at $T \approx 10$ K. Another broadening effect due to the finite bias voltages is shown in Fig. 5 at $T=0$ K. The step structure is somewhat linearized at the small bias voltage[21] and it is thoroughly lineared at $V \geq 2.5$ mV. Two reasons could explain why the finite voltage linearizes $G(\phi)$. One is that $G(\phi)$ at $T=0$ K is related to the difference $[\theta(E-\mu-eV)-\theta(E-\mu)]$ of the two step functions in Eq. (3). The other is that the energy dispersion of the J_a subband is approximately proportional to ϕ. There is no statistical correlation between the broadening effects of

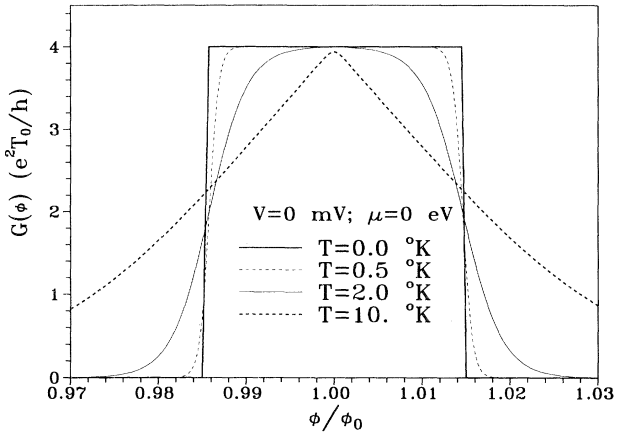

FIG. 4. $G(\phi)$ of the (210,0) nanotube at $V=0$ mV and $\mu=0$ eV, calculated at various temperatures.

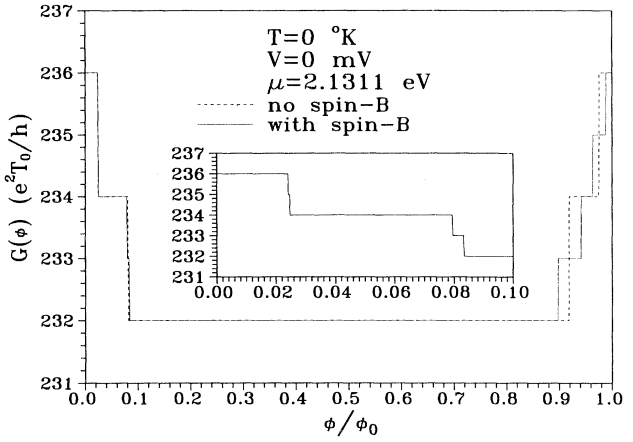

FIG. 6. $G(\phi)$ of the doped (210,0) nanotube at $T=0$ K, $V=0$ mV, and $\mu=2.1311$ eV. The dashed and solid curves, respectively, correspond to those without and with the spin-B interactions. The inset shows the details around the small ϕ's.

the finite temperatures and of the finite bias voltages.[21] The step structures in $G(\phi)$ are thus expected to be observable at $T<1$ K and $V<0.1$ mV, as obtained form Figs. 4 and 5.

For carbon nanotubes with $E_F=0$, the special step structures in $G(\phi)$ are mainly due to the spin-B interaction. Here the Fermi energy increases from zero to a finite value by means of intercalation and our primary concern is to see the roles of the finite Fermi energy and the spin-B interaction in $G(\phi)$. The carbon nanotubes consist of the coaxial graphite layers, which are strongly related to both GIC's and carbon fibers.[19] The charge carries could be introduced into carbon nanotubes by means of intercalation, as done for GIC's and carbon fibers. The alkali-metal atoms[7] are assumed to be intercalated into carbon nanotubes and each carbon atom receives 0.1 e on an average, as found in the stage-one GIC's (C_8M; $M=K$; Rb; Cs). Then, according to the rigid-band model, the Fermi energy is self-consistently determined by the transferred electron density.

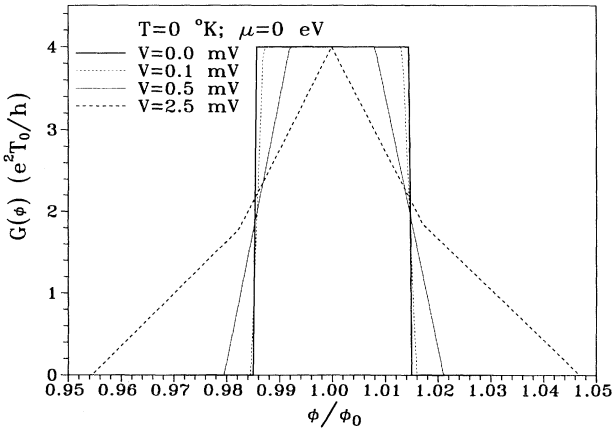

FIG. 5. $G(\phi)$ of the (210,0) nanotube at $T=0$ K and $\mu=0$ eV, calculated at various bias voltages.

We take the doped (210,0) nanotube with $E_F=2.1311$ eV as a model study. $G(\phi)$ of the doped (210,0) nanotube is shown in Fig. 6 at $T=0$ K, $V=0$ mV, and $\mu=2.1311$ eV. The dashed and solid curves, respectively, correspond to the results without and with the spin-B interactions. The results clearly show that there exist four step structures within ϕ_0 even without the spin-B interaction. It implies that the special step structure is caused by the finite Fermi energy (chemical potential). There is one step structure in $G(\phi)$ if one conduction band crosses the Fermi level to become occupied or vacant. There are eight conduction bands (including two spins), for which their band bottoms at $0\le\phi\le\phi_0$ cross E_F, and so there are four step structures with a height of 2 in the absence of the spin-B interaction, as shown by the dashed curve. The step structures possibly happen at a very small B field and their positions mainly depend on the Fermi energy. Here the finite Fermi energy replaces the role of the spin-B interaction in resulting in the step structures. The main effects of the spin-B interaction,[8,9] as shown by the solid curve, are to destroy symmetry (about $\phi_0/2$) and periodicity and double the step structures. The role of the spin-B interaction in the doped nanotube is in sharp contrast to that in the undoped nanotube. There are eight step structures with a height of 1 within ϕ_0 (see the solid curve) for any doped nanotube and more step structures are expected to exist in a doped multiple-shell system, as seen in the undoped case.

In summary, we have calculated the ballistic magnetoconductance of carbon nanotubes. For the undoped nanotubes ($E_F=0$), we predict special step structures in the ballistic magnetoconductance, which are mainly caused by the spin-B interaction. They are expected to be observable at $T<1$ K and $V<0.1$ mV. The tubular system with more shells is more desirable in varying the step structures in $G(\phi)$. The role of the spin-B interaction is

replaced by the Fermi energy for the doped nanotubes, i.e., the finite Fermi energy may also give rise to the step structures. However, the period ϕ_0 of the AB effect is obviously destroyed by the spin-B interaction for both doped and undoped nanotubes.

One of us (M.F.L.) thanks Dr. Ya-Chi Tsai for a critical reading of the manuscript. This work was supported in part by the National Science Council of Taiwan, the Republic of China under Grants Nos. NSC 83-0208-M-007-041 and NSC 84-2112-M-007-018.

[1]S. Iijima, Nature **354**, 56 (1991).
[2]S. Iijima, P. M. Ajayan, and T. Ichihashi, Phys. Rev. Lett. **69**, 3100 (1992); S. Iijima and T. Ichihashi, Nature **363**, 603 (1993); P. M. Ajayan and S. Iijima, *ibid.* **361**, 333 (1993).
[3]M. S. Dresselhauss, G. Dresselhauss, and R. Saito, Phys. Rev. B **45**, 6234 (1992).
[4]J. W. Mintwire, B. I. Dunlap, and C. T. White, Phys. Rev. Lett. **68**, 631 (1992).
[5]N. Hamada, S. I. Sawada, and A. Oshiyama, Phys. Rev. Lett. **68**, 1579 (1992).
[6]R. Saito, M. Fujita, G. Dresselhauss, and M. S. Dresselhauss, Appl. Phys. Lett. **60**, 2204 (1992); Phys. Rev. B **46**, 1084 (1992).
[7]R. A. Jishi and M. S. Dresselhauss, Phys. Rev. B **45**, 11 305 (1992); R. A. Jishi, M. S. Dresselhauss, and G. Dresselhauss, *ibid.* **47**, 16 671 (1993).
[8]P. J. Lin-Chung and A. K. Rajagopal, J. Phys. Condens. Matter **6**, 3697 (1994); Phys. Rev. B **49**, 8454 (1994).
[9]M. F. Lin and K. W.-K. Shung, Phys. Rev. B **48**, 5567 (1993); **47**, 6617 (1993); Chin. J. Phys. **32**, 879 (1994).
[10]W. Tian and S. Datta, Phys. Rev. B **49**, 5907 (1993).
[11]R. Landauer, IBM J. Res. Dev. **1**, 223 (1957); Philos. Mag. **21**, 863 (1970).
[12]S. Das Sarma and S. He, Int. J. Mod. Phys. B **7**, 3375 (1993).
[13]E. N. Bogachek, M. Jonson, R. I. Shekhter, and T. Swahn, Phys. Rev. B **47**, 16 635 (1993).
[14]Y. Meir, N. S. Wingreen, and P. A. Lee, Phys. Rev. Lett. **66**, 3048 (1991).
[15]L. Wang, J. K. Zhang, and A. R. Bishop, Phys. Rev. Lett. **73**, 585 (1994).
[16]B. J. van Wees, H. van Houten, C. W. J. Beenakker, J. G. Williamson, L. P. Kouwenhoven, D. van der Marel, and C. T. Foxon, Phys. Rev. Lett. **60**, 848 (1988).
[17]D. A. Wharam, T. J. Thornton, R. Newbury, M. Pepper, H. Ahmed, J. E. F. Frost, D. G. Hasko, D. C. Peacock, D. A. Ritchie, and G. A. C. Jones, J. Phys. C **21**, L209 (1988).
[18]M. F. Lin and K. W.-K. Shung (unpublished).
[19]M. S. Dresselhauss and G. Dresselhauss, Adv. Phys. **30**, 139 (1981).
[20]P. R. Wallace, Phys. Rev. **71**, 622 (1947).
[21]P. F. Bagwell and T. P. Orlando, Phys. Rev. B **40**, 1456 (1989).